Influence of Ti addition on thermophyscial properties of $Sm_2Ce_2O_7$ oxides

Xiaoge Chen[1], Hongsong Zhang[2,*], Longfei Zhou[2], Bo Ren[2], An Tang[2], Xudan Dang[2]

[1]*School of Civil Engineering, Henan Institute of Engineering, Zhengzhou 451191, P. R. China*
[2]*School of Mechanical Engineering, Henan Institute of Engineering, Zhengzhou 451191, P. R. China*

Abstract

$Sm_2(Ce_{1-x}Ti_x)_2O_7$ (where x = 0, 0.1, 0.3, 0.5) solid solutions were synthesized by conventional solid state re-action method using Sm_2O_3, CeO_2 and TiO_2 as raw reactants. The synthesized powders were pressed into pellets by cold isostatic pressing and pressure-less sintered at 1600 °C for ten hours. Their phase-structure and thermophysical properties were studied. The synthesized samples exhibit single defect fluorite-type struc-ture. Due to the phonon scattering by substitutional atoms, the thermal conductivities of the $Sm_2(Ce_{1-x}Ti_x)_2O_7$ solid solutions decrease with the increasing Ti^{4+} content over the entire temperature range, which are signifi-cantly lower than that of yttrium stabilized zirconia (YSZ). The thermal expansion coefficients of the prepared $Sm_2(Ce_{1-x}Ti_x)_2O_7$ solid solutions also decrease with the increasing Ti^{4+} fraction, which can be attributed to the lower titanium ion radius.

Keywords: *Ti-doped $Sm_2Ce_2O_7$, solid solutions, thermal conductivity, thermal expansion coefficient*

I. Introduction

The yttrium stabilized zirconia (YSZ) thermal barrier coatings have been applied to protect underlying hot-section components of gas turbine engines from the hot gas streams [1]. However, the main defect of YSZ is the limited operating temperature for long-term application due to the inherent phase-transformation and the en-hanced sintering at high temperatures [2,3]. Therefore, exploration of novel candidates for thermal barrier coat-ings is the key challenge for hotter turbine engines. Re-cently, the $A_2B_2O_7$ oxides (where A = La, Nd, Sm, Gd, Dy etc. and B = Zr, Ce) oxides with a pyrochlore-type or a defect fluorite-type structure have attracted intense interest due to their desirable thermophysical proper-ties [4–8]. In recent studies, it has been reported that the thermal conductivities and expansion coefficients of the $A_2B_2O_7$ oxides can be modified by doping with one or more quadrivalent oxides [9–13]. For example, Nd and Ce simultaneous substitution has significant in-fluence on the crystal-structure of $Gd_{2-x}Nd_xZr_{2-y}Ce_yO_7$ solid solutions. The $Gd_{2-x}Nd_xZr_{2-y}Ce_yO_7$ (1.6 ≤ x ≤ 2, 0 ≤ y ≤ 0.4) ceramics have pyrochlore-type struc-ture, while the $Gd_{2-x}Nd_xZr_{2-y}Ce_yO_7$ (0 ≤ x ≤ 2, 0.8 ≤ y ≤ 2) ceramics exhibit a defect-fluorite struc-ture [9]. Wang *et al.* studied the thermal conductiv-ity of $La_2(Zr_{1-x}B_x)_2O_7$ (B = Hf, Ce, 0 ≤ x ≤ 0.5) solid solutions, and found that the size difference domi-nates the phonon scattering by point defects [10]. The $(Sm_{0.5}Gd_{0.5})_2(Ce_{1-x}Zr_x)_2O_7$ ceramics exhibit a defect-fluorite structure, and the thermal expansion coefficients and conductivities decrease gradually with increasing Zr contents [11]. The thermal conductivities and expan-sion coefficients of $Gd_2(Zr_{1-x}Ti_x)_2O_7$ solid solutions de-crease with increasing Ti content [12,13]. Furthermore, several quadrivalent oxides, such as TiO_2, SnO_2 and ThO_2, were also used to reduce the thermal conductivity of Y_2O_3-ZrO_2 [14–16] and $LaMgAl_{11}O_{19}$ [17]. How-ever, there were few reports about the thermophysical properties of $Sm_2(Ce_{1-x}Ti_x)_2O_7$ solid solutions. There-fore, the influence of Ti substitution for Ce on thermo-physcial properties of fluorite-type $Sm_2Ce_2O_7$ was in-vestigated in the current work.

II. Experimental procedure

In the current study, the $Sm_2(Ce_{1-x}Ti_x)_2O_7$ solid solu-tions were prepared by conventional solid state reaction method. Sm_2O_3 (Ruier Advanced Materials Co., Ltd.,

---
*Corresponding author: tel: +86 798 8499000,
e-mail: *zhsandchen@126.com*

China; purity ≥99.9%), CeO_2 (Ruier Advanced Materials Co., Ltd, China; purity ≥99.9%) and TiO_2 (Shenzhen Nanbo Structure Ceramics Co., Ltd, China; purity ≥99.9%) were selected as the precursor powders. Appropriate amounts of Sm_2O_3, CeO_2 and TiO_2 were weighted and mixed fully in an agate mortar, and the resultant powders were pressed into pellets (17 mm diameter and 2 mm thickness) under pressure of 10 MPa, which were further compacted by cold isostatic pressing method at 200 MPa for five minutes. The compacted samples were then pressure-less sintered at 1600 °C for ten hours. The phase constituents of the synthesized samples were identified by X-ray diffraction (XRD, Bruker, D8 Advance, Germany) with CuKα radiation. The RM2000 Raman system (Renishaw RM2000, England) was used to record the Raman spectra of the obtained samples at room temperature.

The actual density measurements of the sintered samples were carried out via the Archimedes principle with deionized water as an immersion medium. In order to observe the microstructure, the sintered samples were polished by diamond paste and were then thermally etched at 1500 °C for 2 h. The field emission scanning electron microscope (SEM, Hitach S-4800, Japan) and energy dispersive X-ray spectrometer were used to analyse the surface microstructure. The Neumann-Kopp rule was employed to calculate the specific heat capacity based on the chemical composition of the sintered samples and the heat capacity data of the constituent elements. The thermal expansion properties of the obtained bulk samples were studied via a high-temperature thermal expansion instrument (Netzsch DIL 801, Germany) between room temperature and 1200 °C. The sample size for thermal expansion measurement was about 3 × 4 × 5 mm. The thermal diffusivity investigation was performed by a laser thermal apparatus (Netzsch LFA 427, Germany) from 200 to 1000 °C. Two thin graphite films were coated on the back and front faces of every sample before measurement. In light of the investigated density, specific heat capacity and thermal diffusivity, the Eq. 1 and Eq. 2 were used to calculate the thermal conductivities of the sintered samples [16,17]:

$$k = C_p \cdot \rho \cdot \lambda \tag{1}$$

$$\frac{k}{k_0} = 1 - \frac{4}{3}\varphi \tag{2}$$

where k, k_0 and φ represent the thermal conductivity, actual thermal conductivity and porosity of the bulk samples.

III. Results and discussion

3.1. Phases and microstructure

XRD patterns of the sintered $Sm_2(Ce_{1-x}Ti_x)_2O_7$ samples were plotted in Fig. 1 together with the data of standard CeO_2. It can be observed that the pure $Sm_2(Ce_{1-x}Ti_x)_2O_7$ solid solutions with single fluorite-
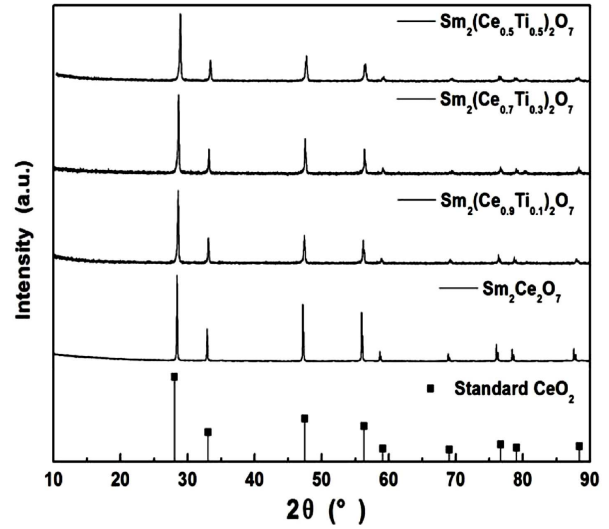

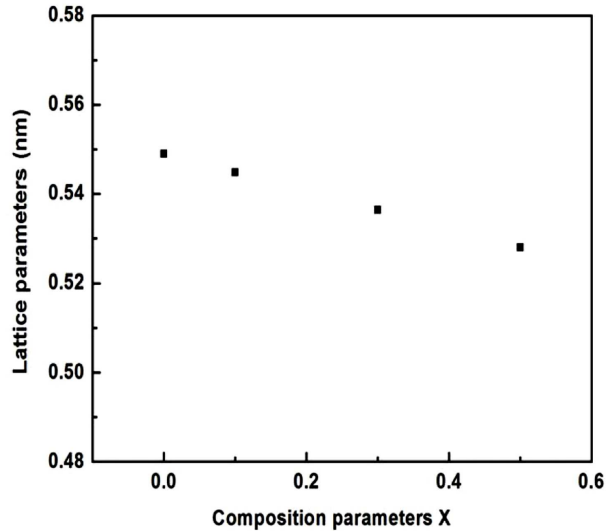**Figure 1. XRD patterns of sintered $Sm_2(Ce_{1-x}Ti_x)_2O_7$ solid solutions**

Figure 2. Lattice parameters of sintered $Sm_2(Ce_{1-x}Ti_x)_2O_7$ solid solutions

type structure were prepared successfully without any XRD peaks of secondary phases. With increasing Ti content, the positions of all reflections shift gradually to the higher angles, which imply that Ce^{4+} ions were substituted partially by Ti^{4+} ions. The calculated lattice parameters for the synthesized samples are depicted in Fig. 2. Clearly, an appropriate linear decrease of the lattice parameters for $Sm_2(Ce_{1-x}Ti_x)_2O_7$ solid solutions can be noted with increasing Ti-content.

For $A_2B_2O_7$-type oxides, the crystal-structure is always determined by the ionic radius ratio of r_A/r_B. In the range of $1.46 \leq r_A/r_B \leq 1.78$, the stable pyrochlore-type oxides can be formed. Below 1.46, the defect fluorite-type oxides can be produced [19,20]. For $Sm_2(Ce_{1-x}Ti_x)_2O_7$ solid solutions, the ionic radii of Sm^{3+}, Ce^{4+} and Ti^{4+} are 0.1079 nm, 0.097 nm and 0.606 nm. The r_A/r_B can be estimated by Eq. 3 in light

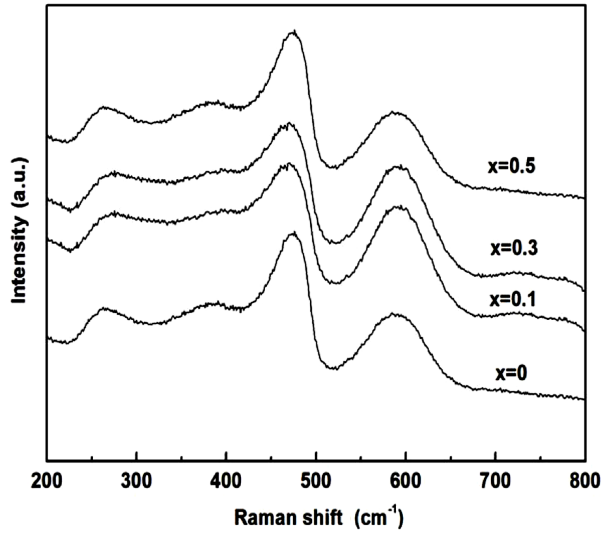**Figure 3. Raman spectra of Sm$_2$(Ce$_{1-x}$Ti$_x$)$_2$O$_7$ solid solutions**

of the ionic radii of the component elements:

$$\frac{r_A}{r_B} = \frac{r(\text{Sm}^{3+})}{(1-x)r(\text{Ce}^{4+}) + xr(\text{Ti}^{4+})} \quad (3)$$

Thus, computed r_A/r_B values of the Sm$_2$(Ce$_{1-x}$Ti$_x$)$_2$O$_7$ solid solutions are 1.11, 1.16, 1.25 and 1.37 for $x = 0$, 0.1, 0.3 and 0.5, respectively. Therefore, the synthesized Sm$_2$(Ce$_{1-x}$Ti$_x$)$_2$O$_7$ solid solutions are expected to exhibit a defect fluorite-type structure, which agrees well with the XRD patterns. Compared with XRD patterns, Raman spectrum is considered to be more sensitive in characterising the structural details and detecting the change of ordering degree of pyrochlore or fluorite [20–24]. As shown in Fig. 3, the Sm$_2$(Ce$_{1-x}$Ti$_x$)$_2$O$_7$ solid solutions have broad Raman bands, which confirms their fluorite structure [20]. The bands at about 380 cm^{-1}, 465 cm^{-1} and 580 cm^{-1} can be attributed to the F_{2g} vibration mode in light of the space group $Fm3m$ of fluorite structure, and the band at about 260–270 cm^{-1} is assigned to the

(a)

(b)

(c)

(d)
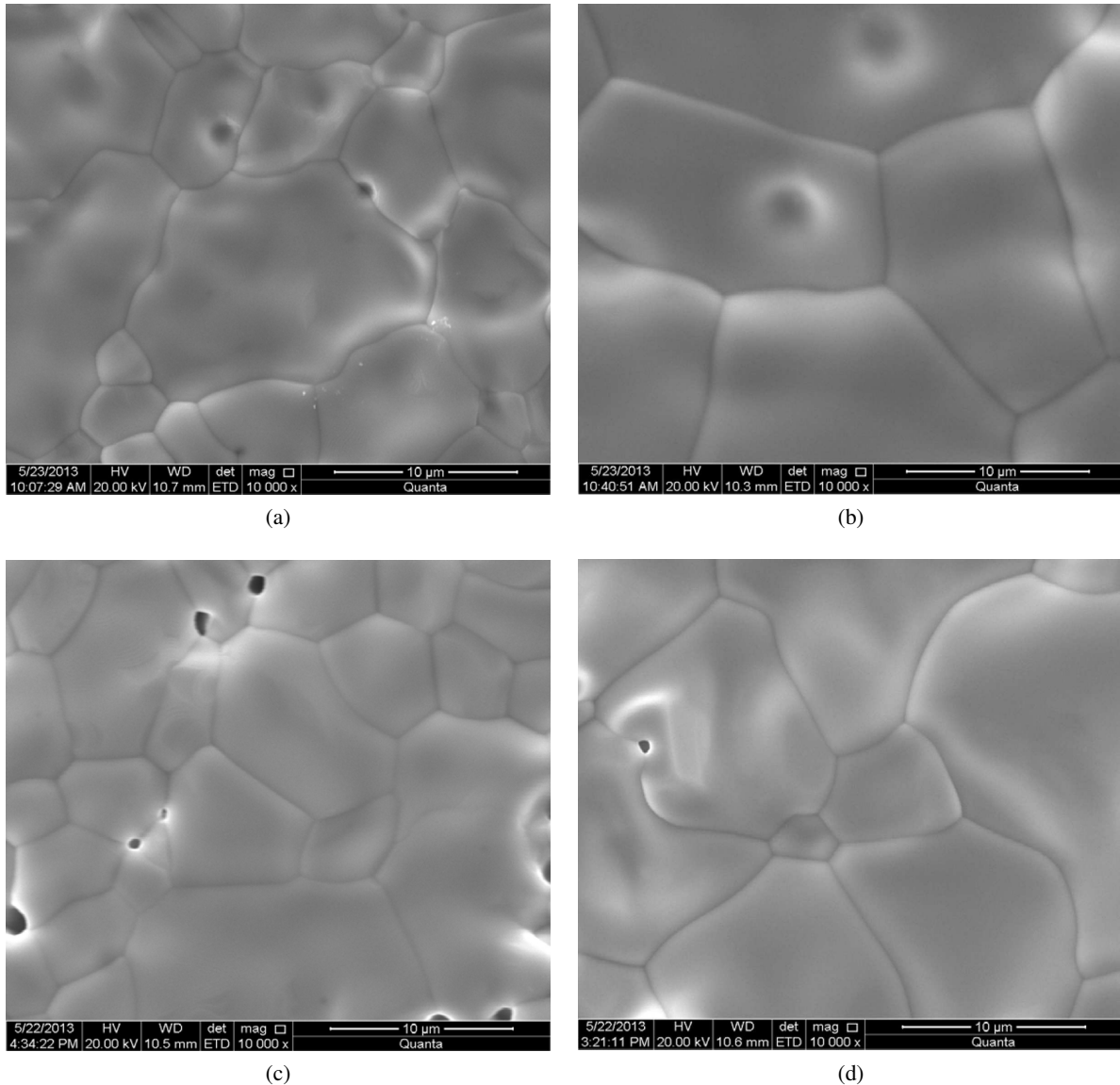
Figure 4. Microstructure of sintered Sm$_2$(Ce$_{1-x}$Ti$_x$)$_2$O$_7$ solid solutions: a) $x = 0$, b) $x = 0.1$, c) $x = 0.3$ and d) $x = 0.5$

E_g mode [21–24]. In these compounds, the broad Raman bands are believed to stem from structural disorder [22], and these high-intensity broad bands are due to the creation of a large number of oxygen vacancies [23]. Thus, the Raman spectra displayed in Fig. 3 further confirmed the possibility of the incorporation of Ti^{4+} into $Sm_2Ce_2O_7$ lattice, which is consistent with the XRD results.

Typical surface morphologies of $Sm_2(Ce_{1-x}Ti_x)_2O_7$ solid solutions with $x = 0.0, 0.1, 0.3$ and 0.5 are exhibited in Fig. 4. Obviously, the dense microstructures with well-defined and closely packed grains can be obtained in all the compositions. The grain size of these solid solutions is several micrometers and the grain interfaces are clean. With the increasing Ti content, relative densities of the $Sm_2(Ce_{1-x}Ti_x)_2O_7$ solid solutions measured by Archimedes principle are 95.4%, 95.8%, 92% and 91.4% of theoretical density for $x = 0, 0.1, 0.3$ and 0.5, respectively.

3.2. Thermal conductivity

The specific heat capacities of the $Sm_2(Ce_{1-x}Ti_x)_2O_7$ solid solutions calculated by Neumann-Kopp rule at various temperatures are plotted in Fig. 5. From Fig. 5, the calculated specific heat capacities are directly proportional to temperature. As the TiO_2 content increases, the calculated specific heat capacities of $Sm_2(Ce_{1-x}Ti_x)_2O_7$ solid solutions firstly decrease, with the minimum value at composition of $x = 0.1$, and then starts increasing, which can be fitted by the following Eq. 4–6:

$$C_p[Sm_2(Ce_{0.9}Ti_{0.1})_2O_7] =$$
$$0.37493 + 0.00009 \times T - 4525.57935 \times T^{-2} \quad (4)$$

$$C_p[Sm_2(Ce_{0.7}Ti_{0.3})_2O_7] =$$
$$0.3954 + 0.00009 \times T - 4935.66579 \times T^{-2} \quad (5)$$

$$C_p[Sm_2(Ce_{0.5}Ti_{0.5})_2O_7] =$$
$$0.41839 + 0.00009 \times T - 5396.11733 \times T^{-2} \quad (6)$$

In the temperature range of 200–1000 °C, the measured thermal diffusivities of the $Sm_2(Ce_{1-x}Ti_x)_2O_7$ solid solutions are displayed in Fig. 6, which are the arithmetic means of three measurements. The error bars were not included in Fig. 6 because they are smaller than the symbols. From Fig. 6, the thermal diffusivities of all the specimens decrease with increasing temperature, which exhibits dominant phonon conduction behaviour as in most polycrystalline materials [23,24]. On the base of thermal diffusivity, density and specific heat capacity, the thermal conductivities of the $Sm_2(Ce_{1-x}Ti_x)_2O_7$ solid solutions were calculated by Eq. 1 and calibrated by Eq. 2, as displayed in Fig. 7. Clearly, Ti addition effectively reduces the thermal conductivity of the pure $Sm_2Ce_2O_7$, and the thermal conductivities of the $Sm_2(Ce_{1-x}Ti_x)_2O_7$ solid solutions at 1000 °C are within the range of 0.75–1.17 W/m·K. The composition with $x = 0.5$ shows the lowest thermal conductivity among all the investigated solid solutions. It is well known that the thermal con-
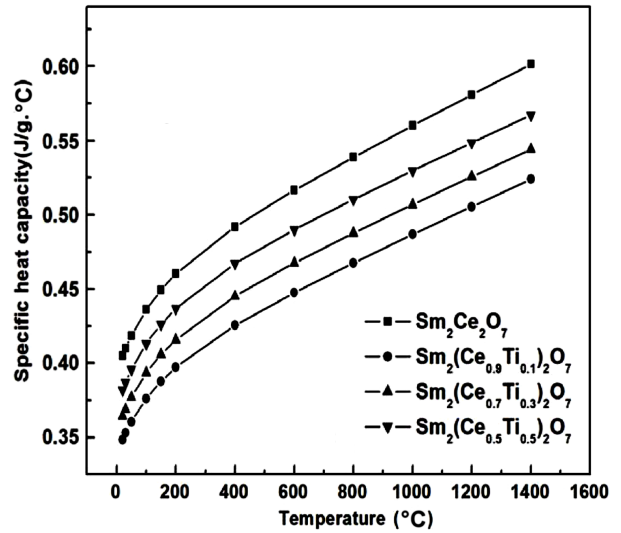

Figure 5. Specific heat capacity of $Sm_2(Ce_{1-x}Ti_x)_2O_7$ solid solutions as a function of temperature
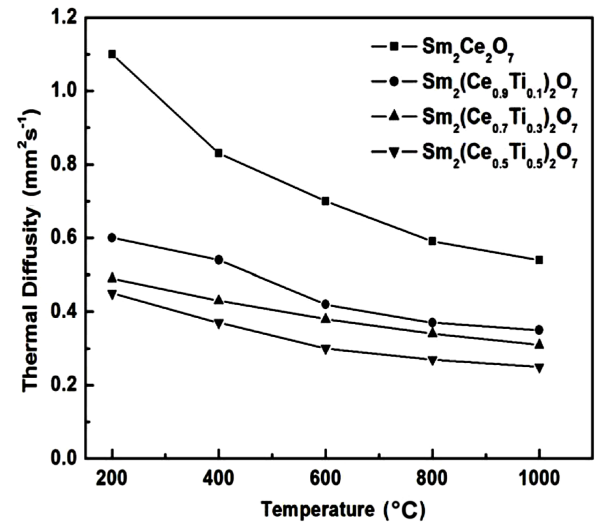

Figure 6. Thermal diffusivity of $Sm_2(Ce_{1-x}Ti_x)_2O_7$ solid solutions as a function of temperature
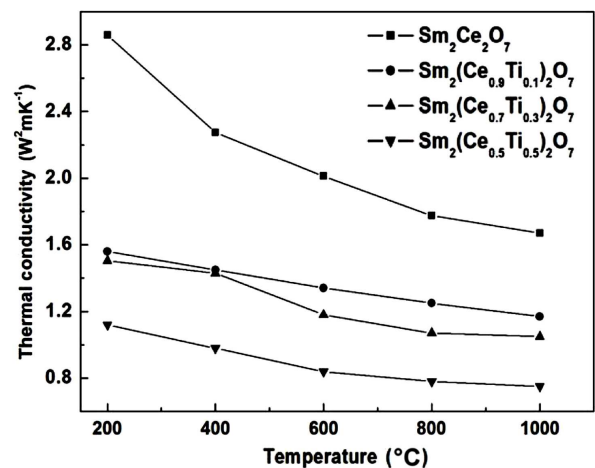

Figure 7. Thermal conductivity of $Sm_2(Ce_{1-x}Ti_x)_2O_7$ solid solutions as a function of temperature

ductivity is proportional to the phonon mean free path. The $Sm_2(Ce_{1-x}Ti_x)_2O_7$ solid solutions were formed by substituting Ti^{4+} for Ce^{4+} in $Sm_2Ce_2O_7$. Due to the significant difference in mass and ionic radius between Ti^{4+} and Ce^{4+}, the substitutional point defects are introduced in $Sm_2Ce_2O_7$, which can increase the phonon scattering and reduce the phonon mean free path [25]. Therefore, the thermal conductivity of the pure $Sm_2Ce_2O_7$ can be reduced by Ti^{4+} doping, and the thermal conductivities of the $Sm_2(Ce_{1-x}Ti_x)_2O_7$ solid solutions are obviously lower than that of YSZ [26].

3.3. Thermal expansion coefficient

Figure 8 plots the thermal expansion rate dependence of the $Sm_2(Ce_{1-x}Ti_x)_2O_7$ solid solutions on temperature. Obviously, the thermal expansion rates of all the samples are linear, which implies that the $Sm_2(Ce_{1-x}Ti_x)_2O_7$ solid solutions have excellent phase stability up to 1200 °C. The relationship between ther-
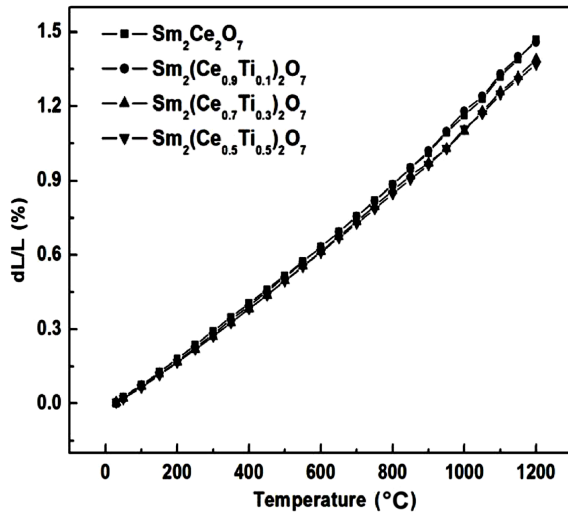

Figure 8. Calibrated dilatometric data of $Sm_2(Ce_{1-x}Ti_x)_2O_7$ solid solutions as a function of temperature

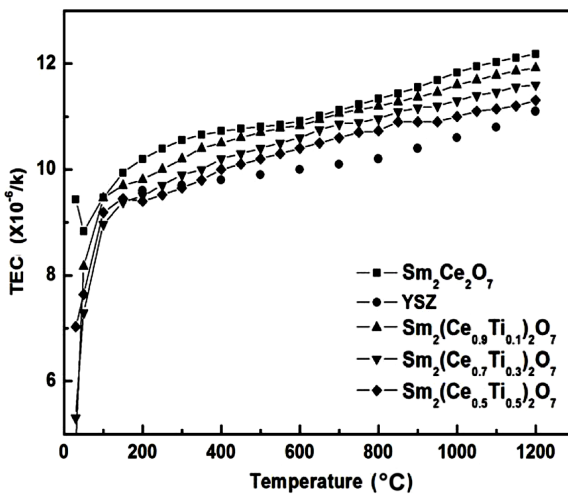**Figure 9. Thermal expansion coefficient of $Sm_2(Ce_{1-x}Ti_x)_2O_7$ solid solutions as a function of temperature**

mal expansion coefficient and temperature for all the bulk samples was presented in Fig. 9. Clearly, owning to the enlarged atomic-distance at high temperatures [27], the thermal expansion coefficients for the $Sm_2(Ce_{1-x}Ti_x)_2O_7$ solid solutions increase with increasing temperature from 20 to 1200 °C. In addition, the Ti-doped $Sm_2Ce_2O_7$ exhibits higher thermal expansion coefficient than YSZ, and the thermal expansion coefficients of $Sm_2(Ce_{1-x}Ti_x)_2O_7$ solid solutions decrease with increasing TiO_2 fraction in the entire temperature range. It is well known that the thermal expansion coefficient varies inversely with crystal energy [28]. As described by Eq. 7, the crystal energy is closely related with the Avogadro's number (N_A), the Madelung constant (A), the ionic charge (z), the ionic charge of an electron (e), the inter-ionic distance (r_0) and the Born exponent (n) [29]:

$$U = \frac{N_A A z^+ z^- e^2}{r_0}\left(1 - \frac{1}{n}\right) \qquad (7)$$

From Eq. 7 it can be deduced that the thermal expansion coefficient is proportional to the inter-ionic distance (r_0), which can be reduced by doping smaller radius Ti^{4+}. Therefore, the thermal expansion coefficients of the $Sm_2(Ce_{1-x}Ti_x)_2O_7$ solid solutions decrease with increasing Ti fraction. The thermal expansion coefficients of the $Sm_2(Ce_{1-x}Ti_x)_2O_7$ solid solutions at 1200 °C are $12.18 \times 10^{-6}\,K^{-1}$, $11.92 \times 10^{-6}\,K^{-1}$, $11.6 \times 10^{-6}\,K^{-1}$ and $11.31 \times 10^{-6}\,K^{-1}$ for $x = 0$, 0.1, 0.3 and 0.5, respectively, which match the requirement for thermal barrier coatings.

IV. Conclusions

The $Sm_2(Ce_{1-x}Ti_x)_2O_7$ solid solutions with single fluorite-type structure were successfully synthesized by conventional solid state reaction method and sintered at 1600 °C. Their thermophysical properties exhibit obvious dependence on the Ti-doping fraction. Due to the enhanced phonon scattering by point defects, the thermal conductivities of the $Sm_2(Ce_{1-x}Ti_x)_2O_7$ solid solutions decrease with the increase in Ti content. The reduced thermal expansion coefficients of all the samples can be attributed to the smaller ion-radius of Ti^{4+}. The synthesized $Sm_2(Ce_{1-x}Ti_x)_2O_7$ solid solutions also exhibit excellent phase-stability up to 1200 °C. The excellent thermophysical properties imply that the $Sm_2(Ce_{1-x}Ti_x)_2O_7$ solid solutions are promising candidate ceramics for thermal barrier coatings.

References

1. M.R.L. Estarki, R.S. Razavi, H. Jamali, R. Ashiri, "Effect of scandia content on the thermal shock behavior of SYSZ thermal sprayed barrier coatings", *Ceram. Inter.*, **42** (2016) 11118–11125.

2. J.H. Perepezko, T.A. Sossaman, M. Taylor, "Ceramic top coat of plasma-sprayed thermal barrier coatings: materials, process and properties", *J. Thermal Spray Technol.*, **26** [5] (2017) 929–940.

3. C. Jing, E.H. Jordan, A.B. Harris, M. Gell, J. Roth, "Double-layer gadolinium zirconate/yttria stabilized zirconia thermal barrier coatings deposited by the solution precursor plasma spray process", *J. Thermal Spray Technol.*, **24** [6] (2015) 895–906.

4. W.X. Ying, G.S. Nan, Z.L. Li, Z. Y. Ping, A. Li, "A novel thermal barrier coating for high-temperature applications", *Ceram. Inter.*, **42** (2016) 2648–2653.

5. L.Z. Guo, Z.W. Heng, O.Y. Jiahu, Z. Yu, "Novel thermal barrier coatings based on rare-earth zirconates/YSZ double-ceramic-layer system deposited by plasma spraying", *J. Alloys Compd.*, **647** (2015) 438–444.

6. H. Zhang, K. Sun, Q. Xu, F. Wang, L. Liu, Y. Wei, X. Chen, "Thermophyscial properties of $Sm_2(Zr_{1-x}Ce_x)_2O_7$ ceramics", *Rare Metals*, **28** [3] (2009) 226–230.

7. Z.H. Song, Y. S. Qing, C.X. Ge, "Preparation and thermophyscial properties of fluorite-type samarium-dysprosium-cerium oxides", *J. Eur. Ceram. Soc.*, **34** (2014) 55–61.

8. G.L. Hua, G.H. Bo, G.S. Kai, X.H. Bin, "Plasma-sprayed $La_2Ce_2O_7$ thermal barrier coatings against calcium-magnesium-alumina-silicate penetration", *J. Eur. Ceram. Soc.*, **34** (2014) 2553–2561.

9. S.S. Jin, D. Yi, S.X. Yan, D. Hui, T. Hong, D.F. Qin, L.X. Rui, "Nd and Ce simutaneous substitution driven modification in $Gd_{2-x}Nd_xZr_{2-y}Ce_yO_7$", *J. Eur. Ceram. Soc.*, **35** (2015) 1847–1853.

10. Y.F. Wang, F. Yang, P. Xiao, "Role and determining factor of substitutional defects on thermal conductivity: a study of $La_2(Zr_{1-x}B_x)_2O_7$ (B = Hf, Ce, $0 \leq x \leq 0.5$) pyrochlore solid solutions", *Acta Mater.*, **68** (2014) 106–115.

11. S.H. Zhang, L. Shi, Y.D. Zhao, "Thermal conductivities and thermal expansion coefficients of $(Sm_{0.5}Gd_{0.5})_2(Ce_{1-x}Zr_x)_2O_7$ ceramics", *J. Mater. Eng. Perform.*, **24** [9] (2015) 3394–3399.

12. L.Z. Guo, O.Y. Jiahu, Z. Yu, X.X. Liang, "Effect of Ti substitution for Zr on the thermal expansion property of fluorite-type $Gd_2Zr_2O_7$", *Mater. Design*, **30** (2009) 3784–3788.

13. L.Z. Guo, O.Y. Jiahu, Z. Yu, X.X. Liang, "Structure and thermal conductivity of $Gd_2(Ti_xZr_{1-x})_2O_7$ ceramics", *Mater. Lett.*, **62** (2008) 4455–4457.

14. Z. Meng, P. Wei, "Effect of lattice defects on thermal conductivity of Ti-doped Y_2O_3-stabilized ZrO_2", *Acta Mater.*, **61** (2013) 5496–5503.

15. M. Zhao, X. Ren, W. Pan, "Low thermal conductivity of SnO_2-doped Y_2O_3-stabilizied ZrO_2: Effect of the lattice tetragonal distortion", *J. Am. Ceram. Soc.*, **98** [1] (2015) 229–235.

16. Z. Meng, R X. Rui, Y. Jun, P. Wei, "Thermo-mechanical properties of ThO_2-doped Y_2O_3 stabilized ZrO_2 for thermal barrier coatings", *Ceram. Inter.*, **42** (2016) 501–508.

17. L.H Ran, W.C. An, Z.C. Guang, "Low thermal conductivity Sr^{2+}, Zn^{2+} and Ti^{4+} ions doped $LaMgAl_{11}O_{19}$ for potential thermal barrier coatings", *Ceram. Inter.*, **40** (2014) 16273–16279.

18. M.A. Subramanian, G. Aravamudan, G.V. Subba Rao, "Oxide pyrochlores-a review", *Prog. Solid State Chem.*, **15** (1983) 55–143.

19. N. Hanako, H. Yamamura, T. Aarai, K. Kakinuma, K. Nomura, "Effect of cation radius ratio and unit cell free volume on oxide-ion conductivity in oxide systems with pyrochlore-type composition", *J. Ceram. Soc. Japan.*, **112** (2004) 541–546.

20. W.X. Zhong, G. Lei, Z.H. Lin, G.S. Kai, G.H. Bo, "Structural evolution and thermal conductivities of $(Gd_{1-x}Yb_x)_2Zr_2O_7$ (x = 0, 002, 0.04, 0.06, 0.08, 0.1) ceramics for thermal barrier coatings", *Ceram. Inter.*, **41** (2015) 12621–12625.

21. M. Glerup, O.F. Nielsen, F.W. Poulsen, "The structure transformation from the pyrochlore structure, $A_2B_2O_7$, to the fluorite structure, AO_2, studied by Raman spectroscopy and defect chemistry modeling", *J. Solid State Chem.*, **160** (2001) 25–32.

22. V.G. Keramidas, W.B. White, "Raman spectra of oxides with the fluorite structure", *J. Chem. Phys.*, **59** (1973) 1561–1562.

23. W.C. Jie, W. Yue, Z.A. Hua, C.Y. Liang, C. Feng, Y. Zhen, "The influence of ionic radii on the grain growth and sintering-resistance of $Ln_2Ce_2O_7$ (Ln = La, Nd, Sm, Gd) ", *J. Mater. Sci.*, **48** (2013) 8133–8139.

24. Z. Yu, G. Lei, Z.X. Xiang, W.C. Mei, Y.F. Xing, "Toughening effect of Yb_2O_3 stabilized ZrO_2 doped in $Gd_2Zr_2O_7$ ceramic for thermal barrier coatings", *Mater. Sci. Eng A.*, **648** (2015) 385–391.

25. Z.X. Qu, C. L. Wan, W. Pan, "Thermal expansion and defect chemistry of MgO-doped $Sm_2Zr_2O_7$", *Chem. Mater.*, **19** (2007) 4313–4318.

26. J. Wu, X. Z. Wei, N.P. Padture, P.G. Klemens, M. Gell, E. García, P. Miranzo, M.I. Osendi, "Low thermal conductivity rare-earth zirconates for potential thermal barrier coating applications", *J. Am. Ceram. Soc.*, **85** [12] (2002) 3031–3035.

27. L. Guo, H.B. Guo, H. Peng, S.K. Gong, "Thermophysical properties of Yb_2O_3 doped $Gd_2Zr_2O_7$ and thermal cycling durability of $(Gd_{0.9}Yb_{0.1})_2Zr_2O_7$/YSZ thermal barrier coatings", *J. Eur. Ceram. Soc.*, **34** (2014) 1255–1263.

28. C.L. Wan, Z.X. Qu, A.B. Du, W. Pan, "Influence of B site substitutional Ti on the structure and thermophysical properties of $A_2B_2O_7$-type pyrochlore $Gd_2Zr_2O_7$", *Acta Mater.*, **57** [16] (2009) 4782–4789.

29. K.V. Govindan Kutty, S. Rajagopalan, C.K. Mathews, "Thermal expansion behaviour of some rare earth oxide pyrochlores", *Mater. Res. Bull.*, **29** (1994) 759–766.